Adaptive mesh refinement based simulations of three-dimensional detonation combustion in supersonic combustible mixtures with a detailed reaction model

Xiaodong Cai[a,b], Jianhan Liang[a,*], Ralf Deiterding[c], Yonggang Che[d], Zhiyong Lin[a],

[a] Science and Technology on Scramjet Laboratory, National University of Defense Technology, 410073, Hunan Changsha.

[b] Institute of Aerodynamics and Flow Technology, German Aerospace Center (DLR), Bunsenstr. 10, 37073 Göttingen, Germany

[c] Aerodynamics and Flight Mechanics Research Group, University of Southampton, Highfield Campus, Southampton SO17 1BJ, United Kingdom

[d] Science and Technology on Parallel and Distributed Processing Laboratory, National University of Defense Technology, 410073, Hunan Changsha, China

Abstract: Detonation combustion initiated with a hot jet in supersonic H_2-O_2-Ar mixtures are investigated by large-scale three-dimensional (3D) simulations in Tianhe-2 computing system with adaptive mesh refinement method. The reactive Euler equations are utilized as the governing equations with a detailed reaction model where the molar ratio of the combustible mixture is 2:1:7 under the condition of pressure 10kPa and temperature 298K. Results show that the Mach stem surface which is formed after the shock surface reflection on the upper wall is actually a local overdriven detonation. The side walls in 3D simulations can play an important role in detonation initiation in supersonic combustible mixtures, because they can help realize triple lines collisions and reflections during the initiation process. The width of the channel has an important influence on the strength of side-wall reflections, and under certain condition there might exist a critical width between the front and back sides of the

Corresponding author. Email addresses: cai-chonger@hotmail.com, jhleon@vip.sina.com, r.deiterding@soton.ac.uk, linzy96@nudt.edu.cn, ygche@nudt.edu.cn

channel for the successful initiation. Both the two-dimensional (2D) and the 3D detonations are overdriven and have a constant but different overdrive after their complete initiations. Although the overdrive degree of the 3D detonation is smaller than that of the 2D case, more complex and irregular detonation fronts can be observed in the 3D case compared with the 2D detonation, which is likely because of the propagation of transverse waves and collisions of triple lines in multi-directions in 3D detonations. After the hot jet is shut down, the newly formed 2D Chapman-Jouguet (CJ) detonation has almost the same characteristic parameters with the corresponding 3D case, indicating that the 2D instabilities can be perfectly preserved in 3D simulations. However, the slapping wave reflections on the side walls in the 3D detonation result in the second oscillation along with the main one, which presents stronger instabilities compared with the 2D case. The inherent stronger 3D instabilities is also verified through the quantitative comparison between the 2D and 3D cases where the 3D result always shows stronger fluctuations than the 2D case.

Keywords: Initiation and propagation, Three-dimensional detonation, Adaptive mesh refinement, Hot jet, Supersonic combustible mixtures

1 Introduction

Scramjet has become one of the first choices in the future in hypersonic propulsion systems because of its superior performance when Mach number exceeds 5[1]. Anyhow, due to its low net thrust, the real applicability of scramjet is still partly limited. Brayton cycle is adopted in scramjet combustors, and its thermodynamic efficiency is much lower than that of detonation combustion[2]. The inherent theoretical advantage of detonation combustion over deflagrative combustion, has promoted the investigations on advanced propulsion of detonation engines[3-5], and therefore the performance of scramjets might be enhanced greatly if detonation combustion is realized in supersonic combustible mixtures in scramjet

combustors.

Reliable initiation methods are one of key issues in detonation investigations. Except for direct initiation[6-9] which can realize initiation immediately but need large energy, an alternative is to use a hot jet that can also realize quick initiation[10]. Researches on detonation initiation with a hot jet have been numerously investigated[11-16], but most of them are carried out only in quiescent combustible mixtures. Detonation initiation and propagation using a hot jet were conducted experimentally by Ishii et al.[17], where the Mach numbers of combustible mixtures were 0.9 and 1.2. Detonation initiation and deflagration to detonation transition (DDT) were investigated experimentally using a hot jet by Han et al.[18][19] in supersonic combustible mixtures, where detonations were directly initiated through shock or shock reflection[20-23] induced by the hot jet. In comparison with experiments, numerical investigations can provide more detailed information. For detonation calculation, additional temporal and spatial scales are introduced by chemical reactions, hence theoretically requiring finer meshes than that of pure flow alone. Considering the computational cost and the resolved resolution, as a compromise the area around the detonation front should be resolved with finer grids where violent reactions are accumulated while relatively coarser grids could be used in the other area. This kind of issue can be properly addressed by structured adaptive mesh refinement (SAMR) framework[24-29]. Based on the DAGH (Distributive Adaptive Grid Hierarchies), the open-code program AMROC (Adaptive Mesh Refinement Object-oriented C++)[30] adopts the SAMR method. It is a sophisticated code and has been validated for parallel numerical simulations of multi-dimensional detonation combustion[31-34].

According to these ideas, a series of adaptive mesh refinement-based simulations on detonation combustions initiated with a hot jet have been conducted in supersonic combustible mixtures[35-38]. The probability of detonation initiation and propagation in

supersonic combustible mixtures was firstly explored through 2D simulations using a simplified reaction model[34] in [35]. Secondly, in order to show its valuable functions for detonation initiation and propagation a systematic research of a hot jet was conducted [36]. Then rather than using the simplified reaction model[34], a detailed reaction model[39] was used in a systematic study investigating the characteristics of detonation initiation using a hot jet[37]. In addition, different from uniform combustible mixtures, detonation initiation and propagation was also conducted in supersonic combustible mixtures with nonuniform velocities[38].

However, detonation combustion is essentially 3D, therefore the full interpretation and understanding of detonation combustion in supersonic combustible mixtures might be limited only through pure 2D simulations. Especially in experiments[18][19] we find that the side walls of the channel might also make an impact on detonation initiation and its propagation, which cannot be investigated only through 2D simulations. While there are undoubtedly similarities between 2D numerical simulations and experimental researches for detonation initiation and propagation in supersonic combustible mixtures[37], the mechanism might be better analyzed and explained with 3D calculations. The simplified reaction models are usually utilized in 3D simulations of detonation combustion[40-47]. However, some fine features which normally characterized by chain-branching reaction processes cannot be resolved through these simplified models. Therefore, a detailed reaction model is necessary to resolve the detailed structure of detonation combustion.

Adaptive mesh refinement-based high-resolution 3D simulations are conducted on detonation initiation and propagation using the detailed reaction model[39], which are part of an ongoing research program for the overall understanding of detonation initiation and its propagation. The paper is organized as follows: the calculation model is given in Section 2.1; the numerical method is shown in Section 2.2; the verification of adaptive mesh refinement is

given in Section 3; detonation initiation is presented in Section 4.1; detonation propagation is presented in Section 4.2; CJ detonation is shown in Section 4.3, and finally Section 5 presents the conclusion of the paper.

2 Calculation model and numerical method

2.1 Calculation model

3D simulations are conducted in a rectangular channel, as depicted in Fig.1. Reflecting boundary conditions are imposed on the four walls, except that a circular inflow with a diameter D_j is embedded within the lower boundary as the model of a hot jet. The inflow condition is adopted on the right boundary while the left boundary imposes the outflow condition. Numerical simulations[48] and experimental observations[49-51] show that there are generally two types of detonation structures. According to the cellular structure regularity, they are usually classified as regular (weakly unstable) and irregular (unstable) structure[52-59]. Compared with regular detonations, irregular detonations need much higher resolutions to be fully resolved numerically[48]. While numerical simulations of unstable detonations can be performed relatively challenging, the simulation of weakly unstable detonations is relatively easily[60]. Considering here the 3D detonation simulations with the detailed reaction model, the regular detonation is preferred in order to precisely resolve the detonation structures while reducing the computational cost. Self-sustaining CJ detonations of H_2-O_2 mixture with a highly argon dilution under a low pressure are ideal choices for detonation simulations because very regular detonations can be generated[61][62]. H_2-O_2-Ar mixture of the molar ratio 2:1:7 with pressure 10kPa and temperature 298K is used as the initial condition of combustible mixtures. The velocity is given the reference CJ velocity V_{CJ}=1627m/s calculated with Cantera[63].

In supersonic combustible mixtures it is much more difficult for 3D detonation initiations than 2D detonation initiations with a hot jet, because in 2D cases the hot jet blocks actually the whole flow. As shown in Table 1, the condition of the hot jet is set to the equilibrium CJ state of H_2/O_2 of the molar ratio of 2:1with pressure 10kPa and temperature 298K, which is calculated using Cantera. In order to make the hot jet as strong as possible, the velocity is given the sonic speed of the equilibrium state to make it a chocked hot jet.

2.2 Numerical method

3D inviscid reactive Euler equations are used as the governing equations with a mixture of different thermally perfect species[30]. For convective flux discretization, a second-order accurate MUSCL-TVD is adopted using finite volume method (FVM). The numerical flux calculation and the reconstruction are used to solve the hydrodynamic process. Compared with Strang splitting, Godunov splitting is employed for 3D numerical simulations because it is computationally more efficient [30]. A hybrid Roe-HLL[30] Riemann solver is adopted to construct inter-cell numerical upwind fluxes, while the Van Albada limiter with MUSCL reconstruction is applied to construct a second-order method in space. As for time integration, second-order MUSCL-Hancock technique[64] is used. The target CFL number 0.95 is adopted together with a dynamic time step adjustment.

It is an interesting point for comparisons between viscous and inviscid detonations. In the simulations solving Euler equations, numerical diffusion is determined by the grid resolution[65]. When the grid resolution is low, physical diffusion is generally dominated by numerical diffusion. Therefore, results solved with Euler and Navier-Stokes equations do not show an obvious difference. However, physical diffusion begins to dominate over numerical diffusion as numerical diffusion decreases when the grid resolution increases. Samtaney and Pullin[66] have discussed this problem comprehensively. High-resolution detonation

simulations using Euler equations can generate unphysical small-scale features resulted from the low numerical diffusion. Nevertheless, qualitative similarities are observed even in high-resolution simulations of viscous and inviscid detonations, especially in regular detonations. Previously Oran et al.[67] conducted a series of viscous and inviscid detonation simulations with detailed reaction model where they observed similar structures in both stable inviscid and viscous detonations, and they indicated that the small-scale structures which are suppressed by numerical diffusion do not have an influence on the entire features of stable detonations. Although diffusion and hydrodynamic instabilities[68-71] are very important for the evolution of irregular detonations, very recently numerical investigations[72-74] showed that from the comparison of the results of Euler and Navier-Stokes equations, diffusion effects have no role in regular detonations due to the absence of hydrodynamic instabilities. Therefore, the conclusions obtained in this paper using Euler equations for regular detonations are nevertheless expected to give at least qualitatively correct descriptions of the detonation features.

3 Verification of adaptive mesh refinement

The length, height and width of the rectangular channel is X=3.2cm, Y=1.6cm, and Z=0.8cm, respectively, as shown in Fig.1. The diameter of the hot jet is D_j=4.0mm, and X_1=1.2cm, Z_1=0.5Z=0.4cm. Under these conditions, the size of detonation cell is λ=1.6cm, therefore a integral detonation cell in the Y direction can be observed in the setup. The base grid is $64\times32\times16$ .The induction length of the one-dimensional ZND (Zel'dovich-von Neumann-Döring) model under these conditions is l_{ig}=0.964mm. The 3D computations are conducted on Tianhe-2 with 1024 Intel E5-2692 2.20 GHz (Ivy Bridge) processors.

It is found that for the detailed reaction[39] considered here, a minimum spatial resolution

of $6\,\mathrm{Pts}/\mathrm{l_{ig}}$ (Points number per induction length) is necessary to accurately resolve all intermediate reaction products in the one-dimensional ZND solution[75]. Around multi-dimensional triple points, a higher resolution is required to capture the internal wave structure completely. The previous 3D verification simulation[31] for the regularly oscillating case uses effective resolution up to $16.8\,\mathrm{Pts}/\mathrm{l_{ig}}$, and the results agree well with that obtained by Tsuboi et al[76] in the same configuration with a uniform grid. The computations here use an effective resolution of $30.85\,\mathrm{Pts}/\mathrm{l_{ig}}$, which can also accommodate the induction length reduction after detonations get overdriven by the injection of the hot jet. This resolution is achieved by five-level refinement with refinement factors 2, 2, 2, 2, respectively. A combination of scaled gradients of pressure, density and temperature and heuristically estimated relative errors in the mass fractions is adopted as adaptive refinement criteria[26].

Fig.2 visualizes temperature contours and the corresponding adaptive level distributions at four different times. In Fig.2(a), a Mach stem is formed after the reflection of the bow shock on the upper wall. It is clearly shown that in the structure of the triple line, there consist of the incident bow shock wave, the Mach stem and the transverse wave (the reflection wave) along with a slip surface behind the triple line. In addition, behind the bow shock surface, there is a combustion surface decoupled with the bow shock. All the features, including the structure of triple line and the combustion surface behind the bow shock, are resolved with the highest refinement level. In Fig.2(b), along the bow shock the Mach stem propagates forward and gradually becomes longer. It is clearly suggested that the dynamic adaptive mesh in the corresponding level distribution has captured precisely the change of the flow. In Fig.2(c), with the further propagation, the flow behind the Mach stem becomes milder shown in the temperature contour, and the refinement level becomes courser to reduce the computational cost. However, in Fig.2(d), the Mach stem becomes unstable resulting in the perturbation behind the Mach stem. Hence, the course mesh in Fig.2(c) is refined again to

adapt the new change.

In this case, these areas where scaled gradients or heuristically estimated relative errors are large can be solved with a high-resolution mesh, while the other areas are coarsely resolved. It is indicated that the criteria for mesh adaption used here can perform very well for the cases. Therefore, the efficiency of high-resolution calculations is improved by decreasing computation costs.

4 Results and analysis

4.1 Detonation initiation

The initiation process of 3D detonation in supersonic combustible mixtures using a hot jet is shown in Fig.3. After the sonic injection of hot jet into the rectangular channel, a bow shock surface is induced by the hot jet in the supersonic flow. This shock surface spreads from the middle to both sides. The shock surface is strongest in the middle line, while it decreases when spreading out to the both sides. During a period of time, the bow shock surface becomes stronger as a whole, and the side shock waves realize the first reflection on the side walls, as shown in Fig.3(a). The reflections on the side walls can enhance the strength of the bow shock surface at the same time, hence the bow shock surface can rise more quickly and reflect on the upper wall. Finally a Mach stem is formed on the upper wall, as shown in Fig.3(b).

The detailed structure of the Mach stem can be observed in Fig.4. Fig.4(a)(c) show that a combustion zone is generated behind the Mach stem. Indicated by the distance between the OH front and Mach stem (presented by the density isoface), the combustion front is coupled with the Mach stem very tightly. In Fig.4(b)(d), it can be obtained that the distance is l=0.714mm , only about three quarters of the theoretical ZND induction length l_{ig} . From the

comparison between Fig.4(a)(b) and Fig.4(c)(d), the Mach stem can propagate towards the supersonic incoming flow with the velocity of V_{CJ}. It is indicated that the Mach stem is actually a locally overdriven detonation.

The Mach stem in Fig.3(c) has propagated forward obviously, and at the same time the triple lines produced by the reflections on the side walls collide together in the horizontal direction. It is shown in Fig.3(c) that a prominent cambered shock surface is generated because of the instantaneous strong heat release after the triple line collision. The Mach stem continues the propagation and finally realizes the first reflection on the lower wall along with the triple lines reflections on the side walls, as shown in Fig.3(d). It can be concluded that during the 3D detonation initiation, the triple lines collisions and triple lines reflections on the surrounding four walls in the channel play an important role in detonation initiation. The triple lines collisions and triple lines reflections can both generate strong shock waves which can realize the auto-ignition of the combustible mixtures immediately and subsequently the instantaneous releasing of the strong chemical energy as the local ignition source, thus in the whole channel resulting in the continuous detonation initiation.

When the width of the channel is increased to Z=1.6cm and the hot jet is still located in the middle of the channel while the other conditions are kept the same, the induced bow shock surface is shown in Fig.5(a). When the shock surface spreads out to both sides, it gets weaker because of the larger width. Although the strength of the wave becomes larger to some degree after the reflections on the side wall as shown from the density pseudocolor in Fig.5(b), it is still not strong enough to enhance the bow shock surface to realize the effective reflection on the upper wall. Finally, detonation initiation is not realized successfully, and the flow keeps stable with the structure of bow shock surface reflection induced by the hot jet. It is indicated that for certain conditions, there should exists a critical distance between the both sides of the channel for the successful initiation. When the distance exceeds the critical value,

there will be not the effective reflection of bow shock surface on the side walls, hence resulting in the failure of detonation initiation.

In 2D simulations of detonation initiation, the hot jet normally blocks the whole flow in real 3D conditions. Therefore, the bow shock will not spread out to the both sides and can maintain the same strength. Nevertheless, the 2D detonation initiation still cannot be realized, and the flow maintains the stable induced bow shock, as shown in Fig.6(a). When the hot jet is newly located at [1.5, 1.9]cm, as shown in Fig.6(b), a shock wave reflection is formed on the upper wall, but the initiation is still not achieved eventually and the flow maintains the stable structure of shock wave reflection all the way. While in 3D cases, the bow shock surface spreads out to both sides and the strength of the bow shock surface will decrease. However, detonation initiation is successfully realized in the 3D case while it fails in the 2D case, indicating that the reflections on the side walls in the 3D case can help prompt the successful detonation initiation for 3D cases. In the 3D simulation, the side walls help realize the triple lines collisions and triple lines reflections, thus having an important influence on detonation initiation in supersonic combustible mixtures, which is different from 2D cases.

4.2 Detonation propagation

After the successful initiation, the initial transverse wave surface propagates between the upper wall and the lower wall until complete detonation combustion is formed in the entire channel. With the help of continuous injection of the hot jet, detonation wave can keep on propagating towards the supersonic incoming flow with the velocity of V_{CJ}, indicating that the detonation wave is actually in an overdriven state.

The overdriven detonation is essentially unstable, which is shown in Fig.7. In Fig.7(a), two groups of triple lines are generated. The group of triple lines on the upper part is beginning to collide with each other. The other group of triple lines on the lower part travels

in an opposite direction and will reflect on the side walls. In Fig.7(b), the two groups of triple lines both realize the collision or reflection. The collisions or reflections of the two triple lines can instantly produce areas of high temperature and pressure as strong initiation sources, resulting in the formation of locally overdriven detonations, as shown in Fig.7(c). Subsequently, the reflections on the front and back walls also generate new transverse wave surfaces and triple lines. The new triple lines propagate between the front and back walls, and finally also form the collisions, generating a newly overdriven detonation in the Z direction. Gradually, more transverse wave surfaces and triple lines are generated in the overdriven detonation because of the essential instability, as shown from Fig.7(d). The propagation of the transverse wave surfaces and the collisions of the triple lines between both Y and Z directions generally result in the complex structures of 3D overdriven detonations.

In the previous 3D detonation simulations in rectangular channels with simplified reaction models or detailed reaction models, the results show different models of detonation fronts: a rectangular mode, a diagonal mode and even a spinning mode[41,43,45,46,77]. However, for the simulation here, none of these detonation modes is observed. For the previous investigations of 3D simulations, the ZND solution is usually used as the initial condition and the CJ detonation can be obtained directly avoiding totally the overdriven state. Nevertheless, because of the presence of the hot jet in the flow field, the initiated detonation is actually in an overdriven state, thus resulting in more complex detonation fronts than the CJ detonation. Different from the results obtained by Williams et al.[78] who conducted a similar simulation of an overdriven detonation using a simplified reaction model, no phaseshift is observed between both Y and Z directions here mainly because of the detailed reaction model adopted.

The reaction fronts in Fig.8(a)(b) are very accidented which can represent the irregularity of the heat release behind the detonation front. The transverse wave surfaces are greatly determined by the heat release, hence resulting in irregular transverse wave surfaces

and triple lines. Fig.8(c)(d) visualizes the 3D variations of induction lengths of the overdriven detonation where the reaction fronts are overlaid by the detonation fronts (represented by the light blue density isofaces). Compared with the reaction fronts in Fig.8(a)(b), the triple lines in Fig.8(c)(d) are always foregoing in both Y an Z directions which indicates that the movement of the triple lines are truly multi-dimensional followed by the reaction fronts.

Fig.9 shows the location histories of the detonation fronts for both the 3D detonation and the corresponding 2D detonation. The corresponding 2D simulation is also conducted at the same time using a stronger hot jet. The hot jet pressure is 1.2 times of that in the 3D cases, and the other conditions all maintain the same. For the 2D case in Fig.9(a), the initiation time (t_i)[37] when detonation initiation is realized is t_{i2d}=46μs, but for the 3D case in Fig.9(b) it is t_{i3d}=230μs which is five times of that in the 2D case. After the successful initiation, the curves are both straight lines for the two cases. The slopes of the lines represent the propagation velocities, suggesting that the detonations keep the same propagation velocities. The propagation velocity in Fig.9(a) is $v = 210.8\text{m/s}$ and in Fig.9(b) is $v = 58.7\text{m/s}$, hence the overdrive degrees for the two cases are $f_{2d} = 1.276$ and $f_{3d} = 1.07$ respectively, where $f = (\frac{v + V_{cj}}{V_{cj}})^2$. The detailed parameters are listed in Table 2.The overdrive degree for the 2D case is a bit larger than that in the 3D case because compared with the 3D case the hot jet actually blocks the whole flow in the 2D case which can make a larger impact on detonation propagation[35]. In addition, after the initiation the line in Fig.9(a) is smooth while it is relatively wiggly in Fig.9(b). Although the only slightly overdriven 3D detonation is not as overdriven as the 2D detonation, it can represent more irregularities which is suggested to be resulted from the inherent instabilities of 3D detonations.

In Fig.10, the detonation fronts are directly visualized when projecting the 3D flow field in the middle of the Z direction to 2D images. Fig.11 shows the numerical schlieren images

for the 2D case. Two relatively regular cells can be observed in the four frames of Fig.11. However, although with quite smaller overdrive degree the induction length in Fig.10 shows significantly larger irregularities and variations compared with the 2D case in Fig.11, and there are hardly any regular cells. The detonation fronts are more complex in 3D cases because of both directions of detonation development than that in the 2D one where the propagation transverse waves and the collision of triple points can be realized only in one direction. However, the induction length in the 2D case keeps the same value of 0.7mm as shown in Fig.11, approximately equal to the mean value (0.714mm) in the 3D case, indicating that the 2D instability can be basically preserved in 3D simulations.

4.3 CJ detonation

Overdriven detonation in supersonic combustible mixtures which stems from the continuous injection of the hot jet[35], requires the support of adequate energy provided by the reactions behind the detonation front. When the hot jet is totally closed, detonation products can expand more freely without the blockage of the hot jet in the flowfield, and then the pressure and temperature behind the detonation wave decrease which subsequently results in the decreasing of the chemical energy release. Therefore, without enough chemical energy releasing it is not possible to continue the propagation of an overdriven detonation. When the overdriven detonation begins to attenuate, the transverse waves become gradually weak which can be absorbed by relatively stronger ones. As a result, the number of triple points decrease and the size of detonation cells grow larger, which can finally result in the formation of stable CJ detonation.

Fig.12 visualizes the periodical location histories of the wave fronts when the CJ detonation is finally formed after shutdown of the hot jet for both the 2D case and the corresponding 3D case. The trochoids are recorded by calculating the point with the maximal

pressure in the middle of the channel. The oscillation periodical for the 2D case in Fig.12(a) is T_{2d}=17.52us, while it is T_{3d}=18.09us for the 3D case in Fig.12(b). Compared with the 2D case, the 3D oscillation periodical is only slightly 3.25% larger, which indicates that the basic 2D instability is basically preserved in the corresponding 3D case while the manifestation in the hydrodynamic flow field is not the same. The velocity of the transverse wave (or transverse surface for the 3D case) is then calculated as Vt_{2d}=913.4m/s and Vt_{3d}=884.36m/s ($Vt=\lambda/T$) respectively, which basically equals to the local sonic speed[79]. The subscript 2d and 3d here represent the 2D case and the 3D case. Compared with the 2D case, the 3D velocity of the transverse surface is slightly 3.18% smaller. The slope of the overall curve shown by the thick arrow represents the relative travelling velocity of detonation wave, which is v_{2d}=22.5m/s and v_{3d}=29.4m/s respectively. Therefore, the absolute propagation velocity should be V_{2d}=1649.5m/s and V_{3d}=1656.4m/s ($V=V_{CJ}+v$). Then the CJ detonation cell length can be calculated as Lc_{2d}=2.89cm and Lc_{3d}=2.99cm ($Lc=T\times V$), respectively, which basically satisfies the formula $\lambda \approx 0.6Lc$ [79]. The detailed parameters are listed in Table 3.

In addition, compared with the 2D case another periodical oscillation with a smaller amplitude is embedded in the main oscillation at the same time as is shown by the thin arrow in Fig.12(b), which indicates that the inherent 3D instabilities are stronger than that of the corresponding 2D case. This weak oscillation has the same periodic with the main oscillation and always occurs in the middle of the main periodical oscillation, which is surmised to be in correlation with the transverse collisions in the horizontal Y direction. Fig.13 shows a series of continuous profiles at the same interval in the horizontal direction from the wall boundary to the center of the flowfield. From the wall to the center of the flowfield, the reaction front represented by the OH isolines is gradually separated from the detonation wave, as shown from Fig.13(a) to Fig.13(c). It is indicated that at this point the detonation is at the attenuation stage. On the other hand, the Mach stem gradually becomes longer from the wall boundary to

the center of the flowfield, suggesting that the reflection of slapping waves on the side walls gradually reaches the center of the flowfield. Finally in Fig.13(d) a new collision in the center of the flowfield is formed and results in the generation of a small bump shown by the blue circle. As shown by the red circle in Fig.13(e), this small bump is actually a new high-pressure zone, where the pressure is approximately 62% higher than that behind the attenuating front. The high-pressure zone can finally induce an abrupt re-initiation behind the attenuating front. It is indicated that the re-initiation initially resulted from the reflection of slapping waves on the side walls generate the relatively weak periodical oscillation. Normally the cellular patterns for 2D detonations miss the slapping waves which are observed in experiments[80], while 3D detonations can actually capture this behavior.

The cellular structures of the 3D CJ detonation are shown in Fig.14, which are mirrored at Z=0.4cm for the visualization of a whole detonation cell. The detonation front on the four side walls presents a quasi-steady periodical rectangular mode and the front displays in turn a convex or a concave, which are essentially 3D and are not the simple overlaps of the corresponding 2D case. In a full detonation cell, the triple lines remain basically parallel to the boundary wall. Fig.15 shows the schematics of triple lines motions deduced from Fig.14. In Fig.14(a), the two triple lines in the Y direction are going to collide with each other while in the Z direction the two triple lines are also advancing to each other with a certain distance, which are simplified in Fig.15(a). Behind the triple lines in the Y direction is the unreacted region which can be totally initiated after the collision of the two triple lines. As shown in Fig.14(b), the initiated unreacted region induces an abrupt detonation. The newly formed triple lines propagate in opposite directions in the Y direction, and in the Z direction the two triple lines are getting closer, preparing for a new collision, which are simplified in Fig.15(b). In Fig.14(c), the two triple lines in the Z direction have realized the collision which initiates a new local detonation. In the Y direction after the reflections on the side walls the two triple

lines both change the propagating direction, as is shown in Fig.15(c). In Fig.14(d), the two triple lines in the Y direction are getting close to each other and prepare for a new collision while in the Z direction after the collision the two triple lines are also propagating to each other, which are simplified in Fig.15(d). The motion of triple lines in Fig.14(d) is similar with that in Fig.14(a), thus forming a complete periodical movement of the cellular structure.

In order to obtain a comparative understanding of 2D and 3D CJ detonation waves, Fig.16 shows the instantaneous pressure and temperature contours of the 2D CJ simulation compared with the pressure and temperature distributions in the middle of the channel of the 3D CJ detonation. For comparison the similar pressure and temperature profiles are selected from the 2D and 3D results. As shown in Fig.16, the overall results of both cases are very similar. A major difference is that the 3D results show a more complex structure behind the detonation front which is actually a keystone-like structure[81][82] as shown in Fig.16(a)(c). This should mainly stem from side-wall reflections discussed previously. In the quantitative comparison, the pressure variations in AA and BB are shown in Fig.17. AA is the middle section of the propagating detonation when the transverse waves just reflected on the side walls, while BB is the middle section when the transverse waves are going to collide with each other. Along AA, the peak pressure and downstream pressure of the 3D results are slightly higher than the 2D results. Because of the collisions between the transverse waves the pressures for both cases rise to a higher level, but the 3D result is still slightly higher than that of the 2D case duo to the side effects as discussed previously. Along BB, the 2D results show peak pressure at the detonation front with a gradual downstream expansion following behind, while a higher peak pressure and a higher downstream pressure are presented in the 3D results, which is different from the previous results[46]. It is indicated that this difference should result from slapping wave reflections on side walls. In addition, both along AA and BB the downstream pressure of the 3D results always shows stronger fluctuations than the 2D

results due to the inherent stronger instabilities of 3D detonation as discussed previously.

5 Conclusion

3D simulations of detonation initiation and propagation using a hot jet in supersonic H_2-O_2-Ar mixtures have been investigated with the detailed reaction model by implementing adaptive mesh refinement method. The corresponding 2D simulations are also conducted for comparisons.

After the reflection of the bow shock surface which is induced by the hot jet on the upper wall and subsequently side walls, a Mach stem surface is formed on the upper wall which is actually a localized overdriven detonation with the reaction zone tightly following behind. From the comparison between the 3D and 2D cases, it is indicated that the side walls in 3D simulations have an important influence on detonation initiation in supersonic combustible mixtures, which can help realize triple lines collisions and reflections during the initiation process. In 2D cases under the same condition, detonation initiation even cannot be realized without the help of the side walls. Under certain condition, there might exist a critical width between the front and back sides of the channel to realize initiation successfully. When the width of the channel is greater than the critical value, effective reflections of the bow shock surface will not be formed successfully on the side walls, hence resulting in the failure of detonation initiation. During the propagation process when the hot jet is ejected continuously, both the 2D and the 3D detonations are overdriven and have a constant but different overdrive. More complex and irregular detonation fronts are observed in the 3D case compared with the 2D detonation, although the overdrive degree of the 3D detonation is smaller than that of the 2D case. Likely because of the propagation of transverse waves and collisions of triple lines in multi-directions, 3D detonation fronts show significantly larger irregularities and variations compared with that of the 2D case. After the shutdown of the hot

jet, the 3D detonation attenuates to CJ detonation as well as the 2D case. The 2D CJ detonation has almost the same characteristic parameters with the 3D case, such as the CJ velocity, transverse wave velocity, oscillating periodic, cell size and so on, indicating that the 2D instabilities can be perfectly preserved in 3D simulations. However, different from the 2D case the slapping wave reflections on the side walls in the 3D detonation result in the second oscillation along with the main one, which presents stronger instabilities compared with the 2D case. The slapping wave exists in the 3D case, which indicates that the inherent 3D instabilities are stronger than that of the corresponding 2D case. This can also be verified through the quantitative comparison of pressure analysis between the 2D and 3D cases where the 3D result always shows stronger fluctuations than the 2D case.

Acknowledgements

This work is supported by National Natural Science Foundation of China under Grant No. 51006119 and Innovative Sustentation Fund for excellent Ph.D. students in National University of Defense Technology under Grant No. B140101. The authors thank sincerely the support from Parallel Visualization Center of School of Computer in National University of Defense Technology for the visualization of 3D large-scale data from Tianhe-2.

Reference

[1] Murthy SNB, Curran ET. High speed flight propulsion systems. Prog Astronaut Aeronaut 1991;137:124-158.

[2] Kailasanath K. Review of propulsion applications of detonation waves. AIAA J 2008;38:1698-1708.

[3] Smirnov NN, Nikitin VF. Modeling and simulation of hydrogen combustion in engines. Int J Hydrogen Energy 2014;39:1122-36.

[4] Smirnov NN, Betelin VB, Shagaliev RM, Nikitin VF, Belyakov IM, Deryuguin YN, Aksenovb SV,

Korchazhkin DA. Hydrogen fuel rocket engines simulation using LOGOS code. Int J Hydrogen Energy 2014;39:10748-56.

[5] Smirnov NN, Nikitin VF, Stamov LI, Altoukhov DI. Supercomputing simulations of detonation of hydrogen-air mixtures. Int J Hydrogen Energy 2015;40:11059-74.

[6] Zhang B, Kamenskihs V, Ng HD, Lee JHS. Direct blast initiation of spherical gaseous detonations in highly argon diluted mixtures. Proc Combust Inst 2011;33:2265-71.

[7] Zhang B, Ng HD, Rémy M, Lee JHS. Critical energy for direct initiation of spherical detonations in H_2/N_2O/Ar mixtures. Int J Hydrogen Energy 2011; 36:5707-16.

[8] Zhang B, Ng HD, Lee JHS. Measurement of effective blast energy for direct initiation of spherical gaseous detonations from high-voltage spark discharge. Shock Waves 2012;22:1–7.

[9] Bane SPM, Shepherd JE, Kwon E, Day AC. Statistical analysis of electrostatic spark ignition of lean H_2/O_2/Ar mixtures. Int J Hydrogen Energy 2011;36:2344-50.

[10] Knystautas R, Lee JHS, Moen I, Wagner HGG. Direct initiation of spherical detonation by a hot turbulent gas jet. Seventeenth Symposium (International) on Combustion 1979;17:1235-45.

[11] Carnasciali F, Lee JHS, Knystautas R, Fineschi F. Turbulent jet initiation of detonation. Combust Flame 1991;84:170-80.

[12] Dorofeev SB, Bezmelnitsin AV, Sidorov VP, Yankin JG, Matsukov ID. Turbulent jet initiation of detonation in hydrogen-air mixtures. Shock Waves 1996;6:73-78.

[13] Medvedev SP, Khomik SV, Olivier H, Polenov AN, Bartenev AM, Gelfand BE. Hydrogen detonation and fast deflagration triggered by a turbulent jet of combustion products. Shock Waves 2005;14:193-203.

[14] Liu SJ, Lin ZY, Liu WD, Lin W, Zhuang FC. Experimental Realization of H_2/Air Continuous Rotating Detonation in a Cylindrical Combustor. Combust Sci Technol 2012;184:1302-17.

[15] Iglesias I, Vera M, Sánchez AL, Liñán A. Numerical analyses of deflagration initiation by a hot jet. Combust Theor Model 2012;16:994-1010.

[16] Carpio J, Iglesias I, Vera M, Sánchez AL, Liñán A. Critical radius for hot-jet ignition of hydrogen–air mixtures. Int J Hydrogen Energy 2013;38:3105-3109.

[17] Ishii K, Kataoka H, Kojima T. Initiation and propagation of detonation waves in combustible high speed flows. Proc Combust Inst 2009;32:2323-30.

[18] Han X, Zhou J, Lin ZY. Experimental investigations of detonation initiation by hot jets in supersonic premixed flows. Chin Phys B 2012;21:124702.

[19] Han X, Zhou J, Lin ZY, Liu Y. Deflagration-to-Detonation transition induced by hot jets in a supersonic premixed airstream. Chin Phys Lett 2013;30:054701.

[20] Gamezo VN, Ogawa T, Oran ES. Flame acceleration and DDT in channels with obstacles: Effect of obstacle spacing. Combust Flame 2008;155:302-15.

[21] Melguizo-Gavilanes J, Rezaeyan N, Lopez-Aoyagi M, Bauwens L. Simulation of shock-initiated ignition. Shock Waves 2010;20:467-78.

[22] Melguizo-Gavilanes J, Bauwens L. Shock initiated ignition for hydrogen mixtures of different concentrations. Int J Hydrogen Energy 2013;38:8061-67.

[23] Melguizo-Gavilanes J, Rezaeyan N, Tian M, Bauwens L. Shock-induced ignition with single step Arrhenius kinetics. Int J Hydrogen Energy 2011;36:2374-80.

[24] Ogawa T, Oran ES, Gamezo VN. Numerical study on flame acceleration and DDT in an inclined array of cylinders using an AMR technique. Comput Fluids 2013;85:63–70.

[25] Berger M. Adaptive mesh refinement for hyperbolic differential equations [Ph.D. thesis]. Stanford, California: Stanford University; 1982.

[26] Berger M, Oliger J. Adaptive mesh refinement for hyperbolic partial differential equations. J Comput Phys 1984;53:484-512.

[27] Crutcheld W, Welcome ML. Object-oriented implementation of adaptive mesh refinement algorithms. J Sci Program 1993;2:145-56.

[28] Friedel H, Grauer R, Marliani C. Adaptive mesh refinement for singular current sheets in incompressible magnetohydrodynamics flows. J Comput Phys 1997;134:190-98.

[29] Neeman HJ. Autonomous hierarchical adaptive mesh refinement [Ph.D. thesis]. Champaign, Illinois: University of Illinois at Urbana-Champaign; 1996.

[30] Deiterding R. Parallel adaptive simulation of multi-dimensional detonation structures [Ph.D. thesis]. Cottbus, Brandenburg: Brandenburg University of Technology; 2003.

[31] Deiterding R. High-Resolution numerical simulation and analysis of Mach reflection structures in detonation waves in low-pressure H_2-O_2-Ar mixtures: A summary of results obtained with the adaptive mesh refinement framework AMROC. J combust 2011;2011.

[32] Deiterding R. A parallel adaptive method for simulating shock-induced combustion with detailed chemical kinetics in complex domains. Comput Struct 2009;87:769-83.

[33] Liang Z, Browne S, Deiterding R, Shepherd JE. Detonation front structure and the competition for radicals. Proc Combust Inst 2007;31:2445-53.

[34] Ziegler JL, Deiterding R, Shepherd JE, Pullin DI. An adaptive high-order hybrid scheme for compressive, viscous flows with detailed chemistry. J Comput Phys 2011;230:7598-630.

[35] Cai XD, Liang JH, Lin ZY, Deiterding R, Qin H, Han X. Adaptive mesh refinement–based numerical simulation of detonation initiation in supersonic combustible mixtures using a hot jet. ASCE J Aerosp Eng 2015;28:04014046.

[36] Liang JH, Cai XD, Lin ZY, Deiterding R. Effects of a hot jet on detonation initiation and propagation in supersonic combustible mixtures. Acta Astronaut 2014;105:265-77.

[37] Cai XD, Liang JH, Lin ZY, Deiterding R, Liu Y. Parametric study of detonation initiation using a hot jet in supersonic combustible mixtures. Aerosp Sci Tech 2014;39:442-55.

[38] Cai XD, Liang JH, Lin ZY, Deiterding R, Zhuang FC. Detonation initiation and propagation in nonuniform supersonic combustible mixtures. Combust Sci Tech 2015;187:525-536.

[39] Westbrook CK. Chemical kinetics of hydrocarbon oxidation in gaseous detonations. Combust Flame 1982;46:191-210.

[40] Williams DN, Bauwens L, Oran ES. Detailed structure and propagation of three-dimensional detonations. Proc Combust Inst 1996;26:2991-98.

[41] Deledicque V, Papalexandris MV. Computational study of three-dimensional gaseous detonation structures. Combust Flame 2006;144:821-37.

[42] Wang C, Lu J, Ye T. Numerical simulation of three-dimensional gas detonation. J Phys 2008;96:012029.

[43] Dou HS, Tsai HM, Khoo BC, Qiu JX. Simulations of detonation wave propagation in rectangular ducts using a three-dimensional WENO scheme. Combust Flame 2008;154:644-59.

[44] Huang Y, Ji H, Lian FS, Tang H. Three-dimensional parallel simulation of formation of spinning detonation in a narrow square tube. Chin Phys Lett 2012;29:114701.

[45] Wang C, Shu CW, Han WH, Ning JG, High resolution WENO simulation of 3D detonation waves. Combust Flame 2013;160:447-62.

[46] Cho DR, Won SH, Shin JR, Choi JY. Numerical study of three-dimensional detonation wave dynamics in a circular tube. Proc Combust Inst 2013;34:1929-37.

[47] Frolov SM, Dubrovskii AV, Ivanov VS. Three-dimensional numerical simulation of operation process in rotating detonation engine. Progr Propul Phys 2013;4:467-88.

[48] Mahmoudi Y, Mazaheri K. High resolution numerical simulation of the structure of 2-D gaseous detonations. Proc Combust Inst 2011;33:2187-94.

[49] Radulescu MI, Lee JHS. The failure mechanism of gaseous detonations: experiments in porous wall tubes. Combust Flame 2002;131:29-46.

[50] Radulescu MI, Sharpe GJ, Lee JHS, Kiyanda CB, Higgins AJ, Hanson RK. The ignition mechanism in irregular structure gaseous detonations. Proc Combust Inst 2005;30:1859-67.

[51] Shepherd JE. Detonation in gases. Proc Combust Inst 2009;32:83-98.

[52] Radulescu MI, Sharpe GJ, Law CK, Lee JHS. The hydrodynamic structure of unstable cellular detonations. J Fluid Mech 2007;580:31-81.

[53] Gamezo VN, Desbordes D. Oran ES. Formation and evolution of two-dimensional cellular detonations. Combust Flame 1999;116:154-65.

[54] Sharpe GJ, Falle SAE. Two-dimensional numerical simulations of idealized detonations. Proc R Soc Lond A 2000;456:2081-2100.

[55] Mach P, Radulescu MI. Mach reflection bifurcations as a mechanism of cell multiplication in gaseous detonations. Proc Combust Inst 2010;33:2279-85.

[56] Hu XY, Khoo BC, Zhang DL, Jiang ZL. The cellular structure of a two-dimensional $H_2/O_2/Ar$ detonation wave. Combust Theory Model 2004;8:339-59.

[57] Hu XY, Zhang DL, Khoo BC, Jiang ZL. The structure and evolution of a two-dimensional $H_2/O_2/Ar$ cellular detonation. Shock Waves 2005;14:37-44.

[58] Mahmoudi Y, Mazaheri K. Triple point collision and hot spots in detonations with regular structure. Combust Sci Tech 2012;184:1135-51.

[59] Mével R, Davidenko D, Austin JM, Pintgen F, Shepherd JE. Application of a laser induced fluorescence model to the numerical simulation of detonation waves in hydrogen-oxygen-diluent mixtures. Int J Hydrogen Energy 2014;39:6044-60.

[60] Mével R, Davidenko D, Lafosse F, Chaumeix N, Dupré G, Paillard CÉ, Shepherd JE. Detonation in

hydrogen–nitrous oxide–diluent mixtures: An experimental and numerical study. Combust Flame 2015;162:1638-49.

[61] Strehlow RA. Gas pase detonations: Recent developments. Combust Flame 1968;12:81-101.

[62] Taylor BD, Kessler DA, Gamezo VN, Oran ES. Numerical simulations of hydrogen detonations with detailed chemical kinetics. Proc Combust Inst 2013;34:2009-16.

[63] Goodwin D. Tech. Rep. California Institute of Technology, http://www.cantera.org.

[64] Leer BV. On the relation between the upwind-differencing schemes of Godunov, Engquist–Osher and Roe. SIAM J Sci Statist Comput 1984;5:1-20.

[65] Sharpe GJ, Transverse waves in numerical simulations of cellular detonations. J Fluid Mech 2001;447:31-51.

[66] Samtaney R, Pullin DI. On initial-value and self-similar solutions of the compressible Euler equations. Phys Fluids 1996;8:2650-55.

[67] Oran E.S., Jr JWW, Stefaniw EI, Lefebvre MH, Jr JDA. A numerical study of a two-dimensional H_2-O_2-Ar detonation using a detailed chemical reaction model. Combust Flame 1998;113:147-63.

[68] Mazaheri K, Mahmoudi Y, Sabzpooshani M, Radulescu MI. Experimental and numerical investigation of propagation mechanism of gaseous detonations in channels with porous walls. Combust Flame 2015;162:2638-59.

[69] Mahmoudi Y, Mazaheri K. High resolution numerical simulation of triple point collision and origin of unburned gas pockets in turbulent detonations. Acta Astronaut 2015;115:40-51.

[70] Emami S, Mazaheri K, Shamooni A, Mahmoudi Y. LES of flame acceleration and DDT in hydrogen-air mixture using artificially thickened flame approach and detailed chemical kinetics. Int J Hydrogen Energy 2015;40:7395-408.

[71] Maxwell BM, Tawagi P, Radulescu MI. The role of instabilities on ignition of unsteady hydrogen jets flowing into an oxidizer. Int J Hydrogen Energy 2013;38:2908-18.

[72] Mazaheri K, Mahmoudi Y, Radulescu MI. Diffusion and hydrodynamic instabilities in gaseous detonations. Combust Flame 2012;113:2138-54.

[73] Mahmoudi Y, Mazaherin K, Parvar S. Hydrodynamic instabilities and transverse waves in propagation mechanism of gaseous detonations. Acta Astronaut 2013;91:263-82.

[74] Mahmoudi Y, Karimi N, Deiterding, Emami S. Hydrodynamic instabilities in gaseous detonations:

Comparison of Euler, Navier–Stokes, and Large-Eddy simulation. J Propul Power 2014;30:384-96.

[75] Deiterding R, Bader G. High-resolution simulation of detonations with detailed chemistry. Analysis and Numerics for Conservation Laws 2005;2005:69-91.

[76] Tsuboi N, Katoh S, Hayashi AK. Three-dimensional numerical simulation for hydrogen/air detonation: Rectangular and diagonal structures. Proc Combust Inst 2002;29:2783-88.

[77] Eto K, Tsuboi N, Hayashi AK. Numerical study on three-dimensional C-J detonation waves: detailed propagating mechanism and existence of OH radical. Proc Combust Inst 2005;30:1907-13.

[78] Williams DN, Bauwens L, Oran ES. Detailed structure and propagation of three-dimensional detonations. Proc Combust Inst 1997;26:2991-98.

[79] Lee JHS. Dynamic parameters of gaseous detonation. Ann Rev Fluid Mech 1984;16:311-36.

[80] Hanana M, Lefebvre MH, Tiggelen PJV. Pressure profiles in detonation cells with rectangular and diagonal structures. Shock Waves 2001;11:77-88.

[81] Pintgen F, Eckett CA, Austin JM, Shepherd JE. Direct observations of reaction zone structure in propagating detonations. Combust Flame 2003;133:211-29.

[82] Sanderson SR, Austin JM, Liang Z, Pintgen F, Shepherd JE, Hornung HG. Reactant jetting in unstable detonation. Prog Aerosp Sci 2010;46:116-31.

Table 1

The equilibrium CJ state of H_2 and O_2 with a molar ratio of 2:1, 298K, 10kPa. Note that the parameters for the nine species are given the mass fractions

Parameters	Values	Unit
Pressure	172718.0558	Pa
Temperature	3269.0376	K
Density	0.08927	kg/m^3
Velocity	1501.0624	m/s
Energy	159548.0785	J/m^3
H_2	0.024077635865217	
H	0.007595184679829	
O	0.053242033018869	
O_2	0.121585060854123	
OH	0.162516631934541	
H_2O	0.630832382085583	
HO_2	0.000141912825712	
H_2O_2	0.000009158736126	
Ar	0	

Table 2

The characteristic parameters of the overdriven detonations for the two-dimensional and three-dimensional cases.

	t_i	v	f
2D	46μs	210.8m/s	1.276
3D	230μs	58.7m/s	1.07

Table 3

The characteristic parameters of the CJ detonations for the two-dimensional and three-dimensional cases.

	T	Vt	V	Lc
2D	17.52us	913.14m/s	1649.5m/s	2.89cm
3D	18.09us	884.36m/s	1656.4m/s	2.99cm

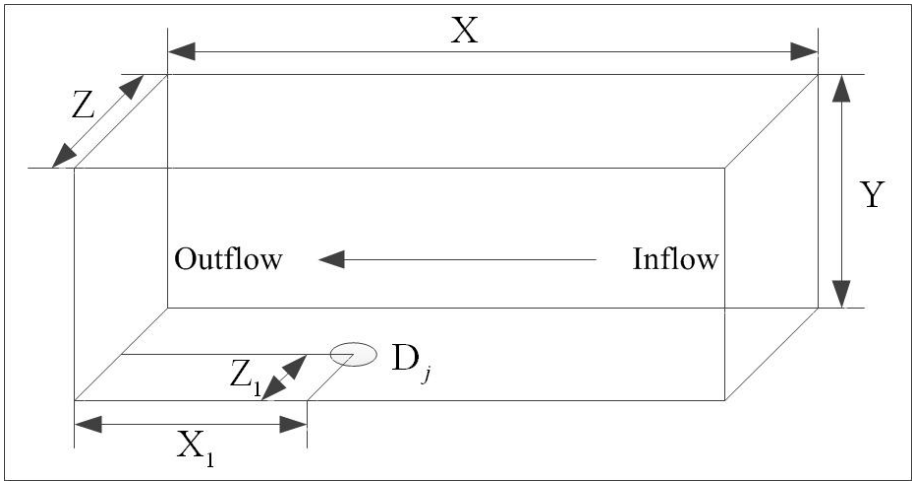

Fig.1 Schematic of the calculation model

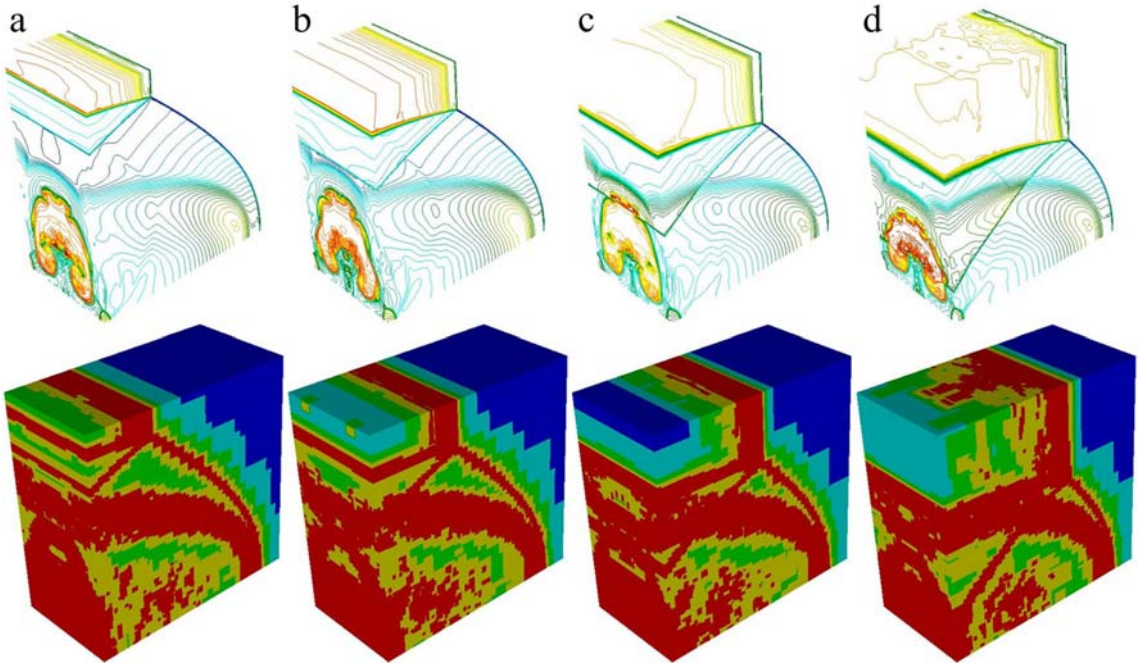

Fig.2 Temperature contours (upper) and the corresponding adaptive level distributions (lower). The mesh adaptation is five-level refinement represented by five different colors. The red color shows the highest fifth refinement level, and the blue color shows the base level. (a) t=234.1μs , (b) t=253.32μs , (c) t=272.78μs , (d) t=292.455μs

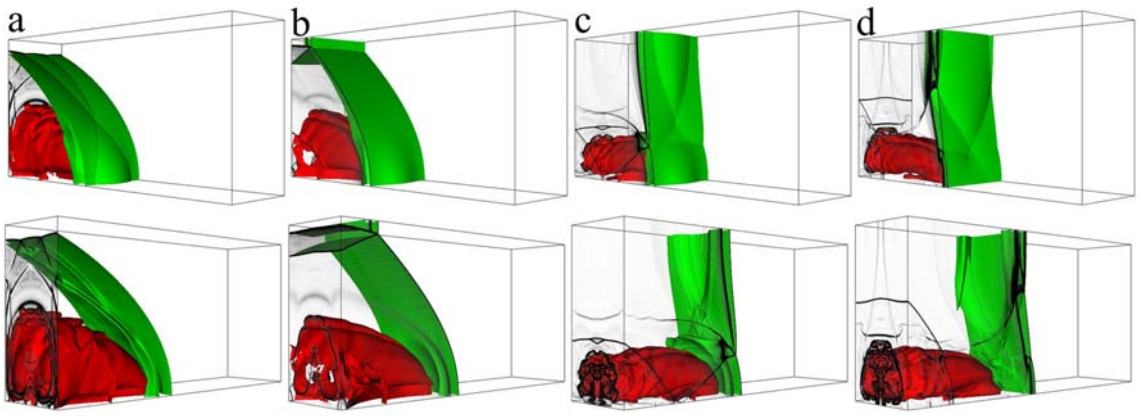

Fig.3 Front view (upper) and rear view (lower) of density isofaces and numerical schlieren images showing the initiation process using a hot jet in the three-dimensional channel. The green density isoface is at a density of $0.3\,\mathrm{kg/m^3}$. (a) t=18.85μs, (b) t=224.34μs, (c) t=323.07μs, (d) t=334.1μs

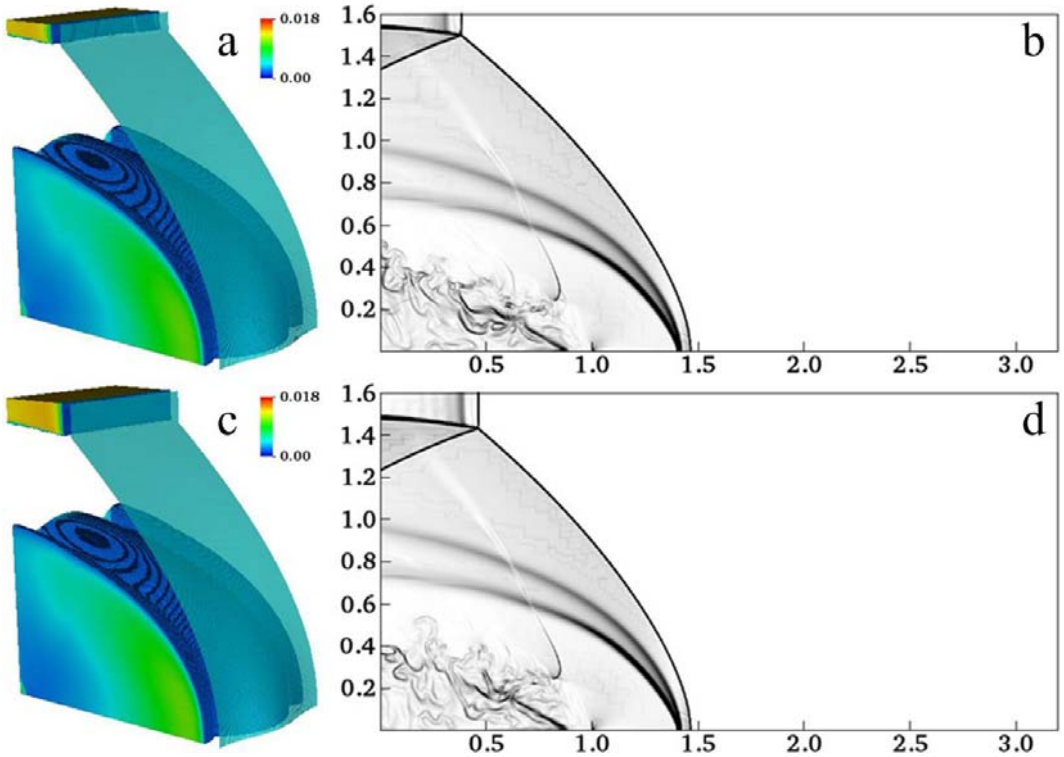

Fig.4 The OH mass fraction pseudocolors and the density isofaces (left) and the numerical schlieren images vertical to Z direction in the channel center (right). The light blue density

isoface is at the density of $0.3\,kg/m^3$. (a)(b) t=224.34μs, (c)(d) t=234.1μs

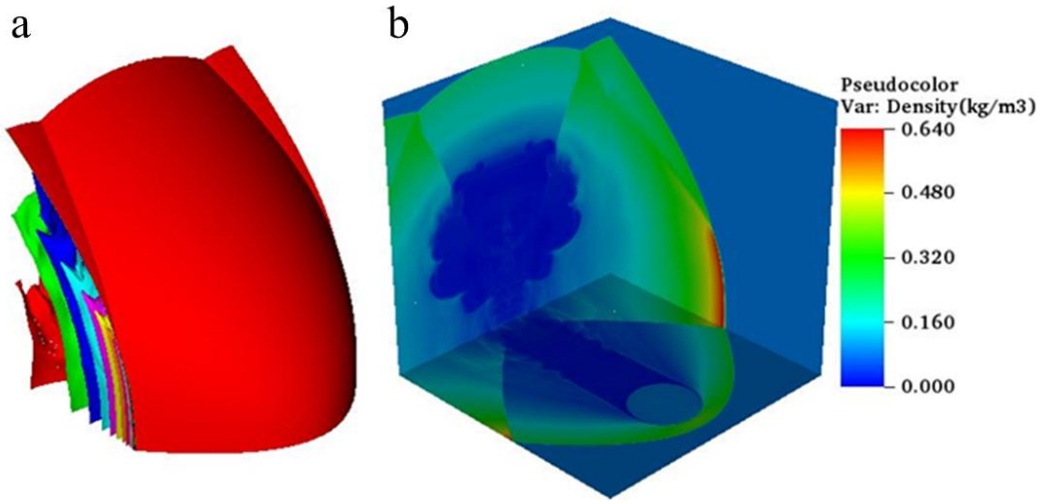

Fig.5 The temperature isoface (a) and the density pseudocolor (b) showing the stable bow shock surface when Z=1.6cm

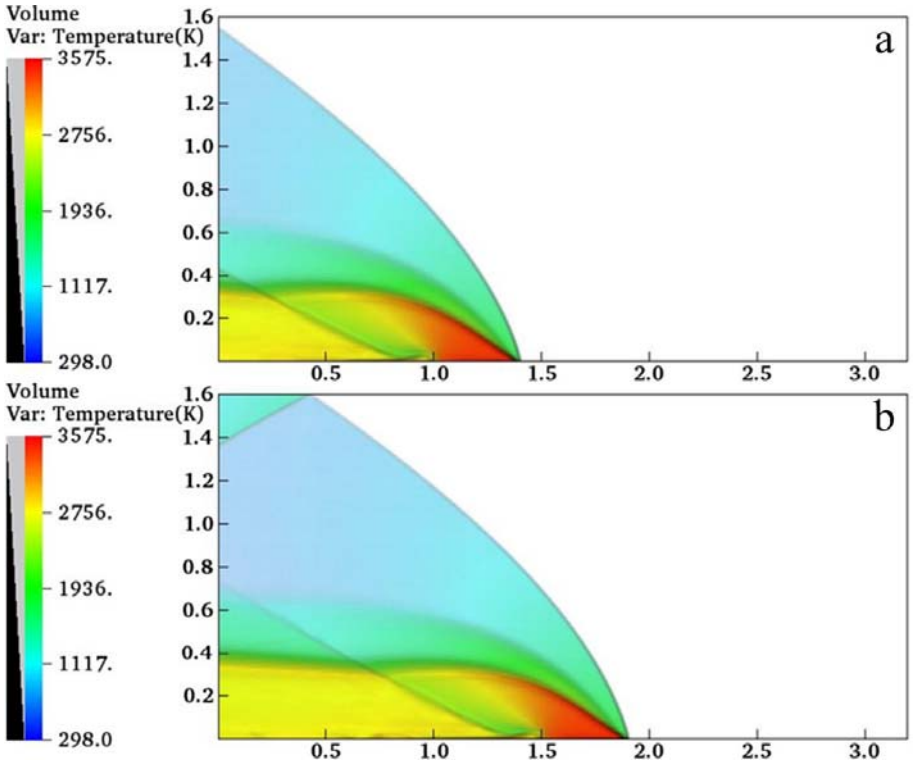

Fig.6 Two-dimensional induced shock reflections for two different locations of hot jet. (a)

[1.0, 1.4]cm, (b) [1.5, 1.9]cm

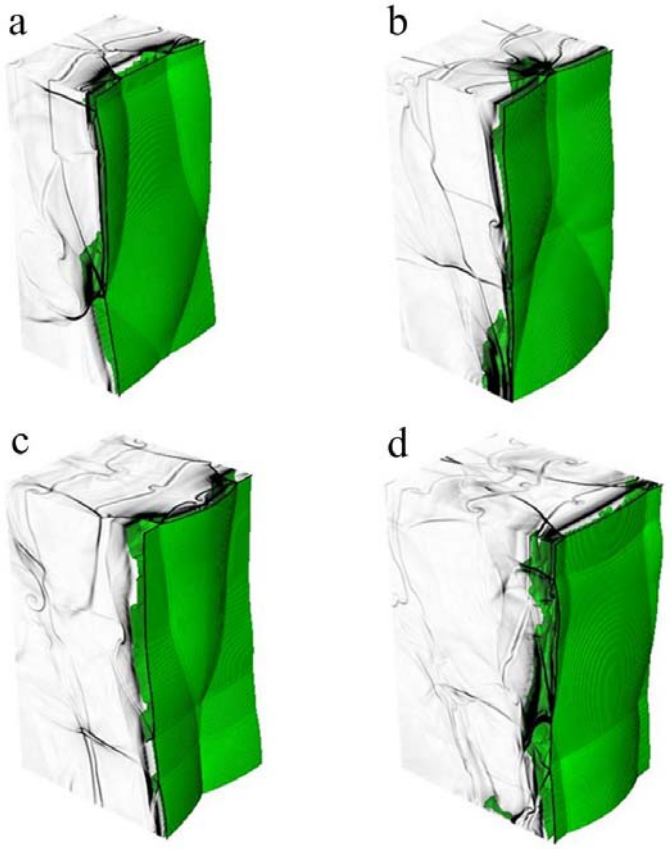

Fig.7 Overdriven detonation shown by the density isofaces at a density of $0.3\,\mathrm{kg/m^3}$ and numerical schlieren images. (a) t=345.35μs , (b) t=356.68μs , (c) t=368.34μs , (d) t=380.07μs

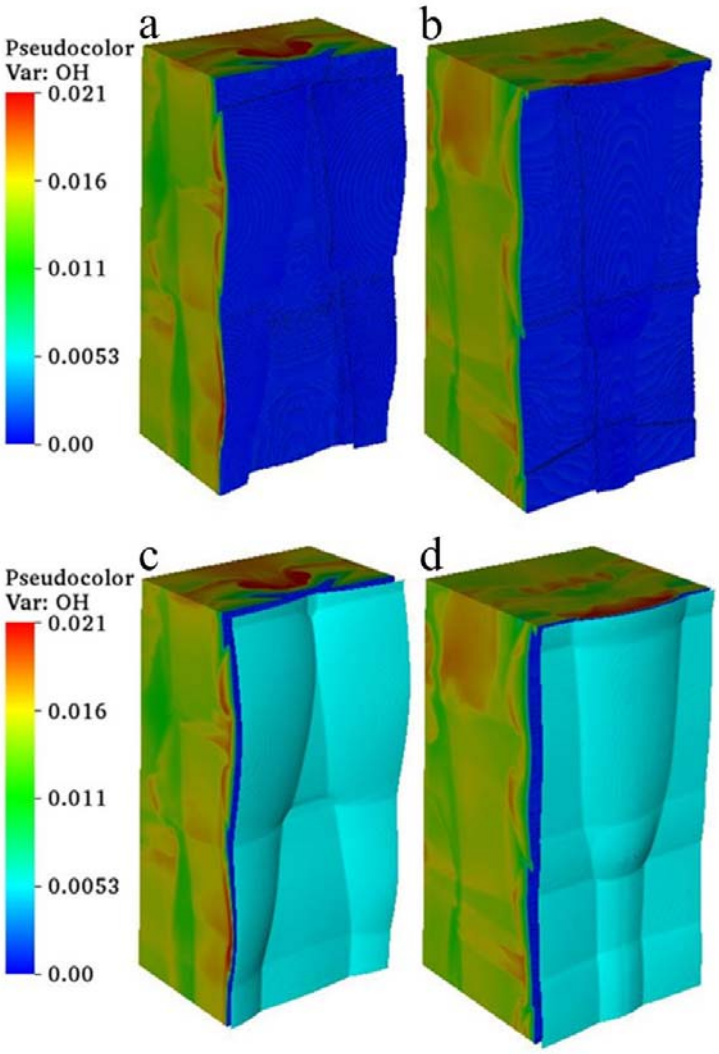

Fig.8 The reaction front represented by the OH mass fractions pseudocolors and the induction zone shown by the OH mass fraction pseudocolors and density isofaces at a density of $0.3\,\mathrm{kg/m^3}$. (a)(c) t=391.84μs, (b)(d) t=403.77μs

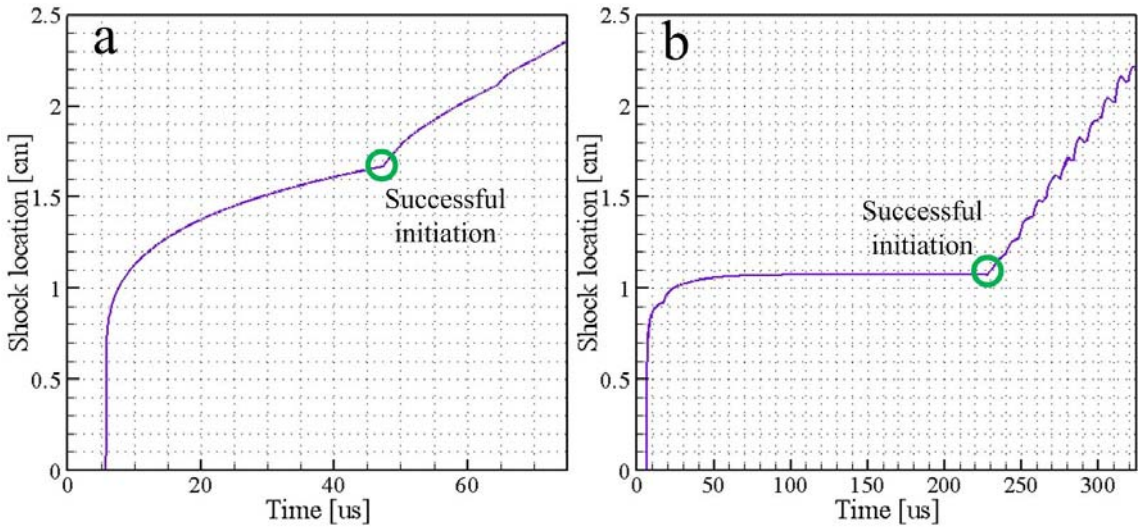

Fig.9 The curves of the shock front locations. (a) Two-dimensional detonation propagation; (b) Three-dimensional detonation propagation

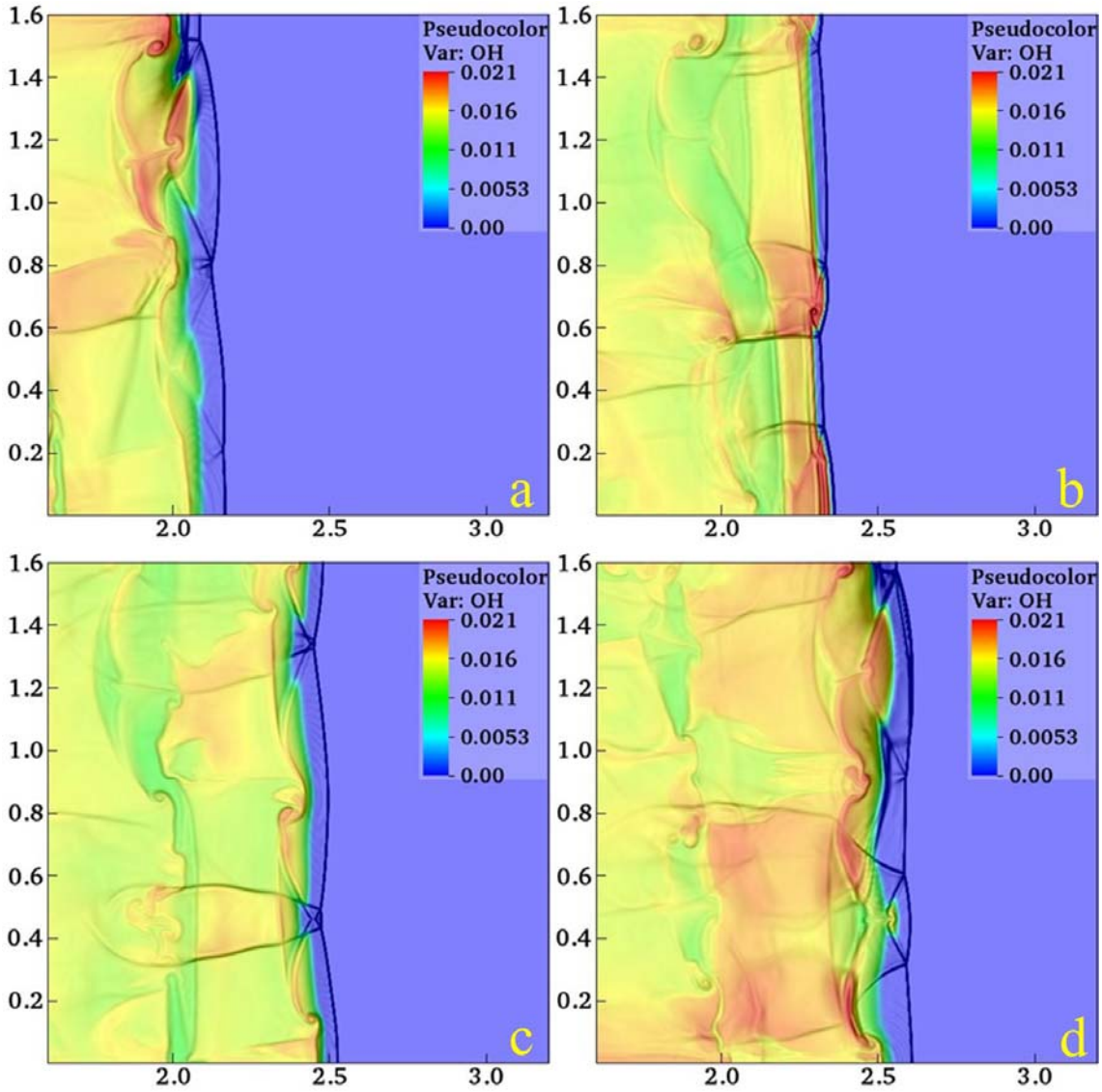

Fig.10 Numerical schlieren images and the corresponding OH mass fraction pseudocolors vertical to Z direction in the channel center. (a) t=391.84μs, (b) t=403.77μs, (c) t=415.74μs, (d) t=427.72μs

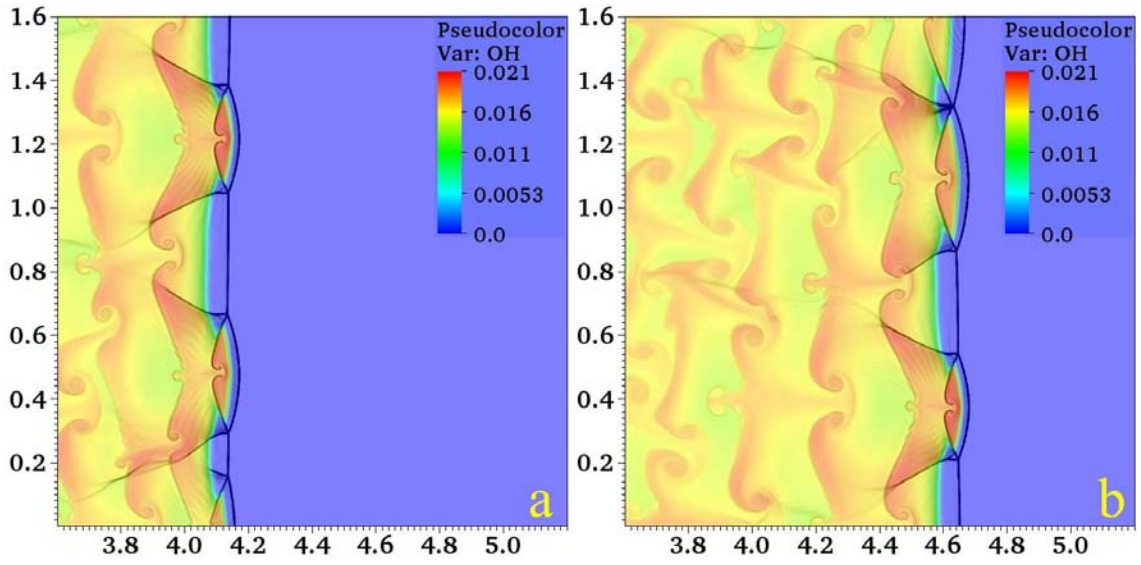

Fig.11 Numerical schlierens and OH contrours showing the patterns of overdriven detonation for the corresponding two-dimensional detonation. (a) t=161.13μs , (b) t=185.48μs

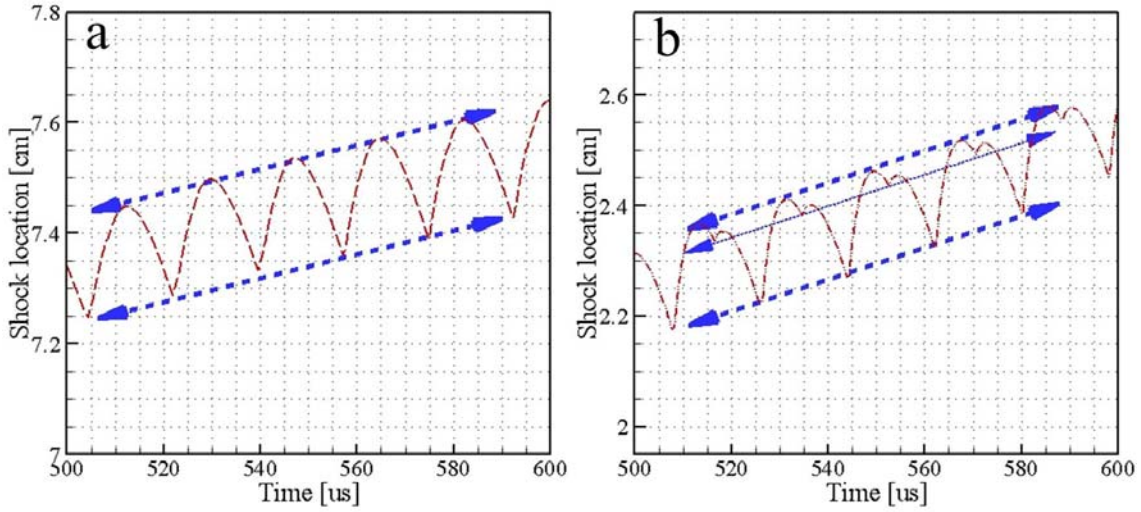

Fig.12 Location histories of CJ detonation fronts for the two-dimensional (a) and three-dimensional detonation (b)

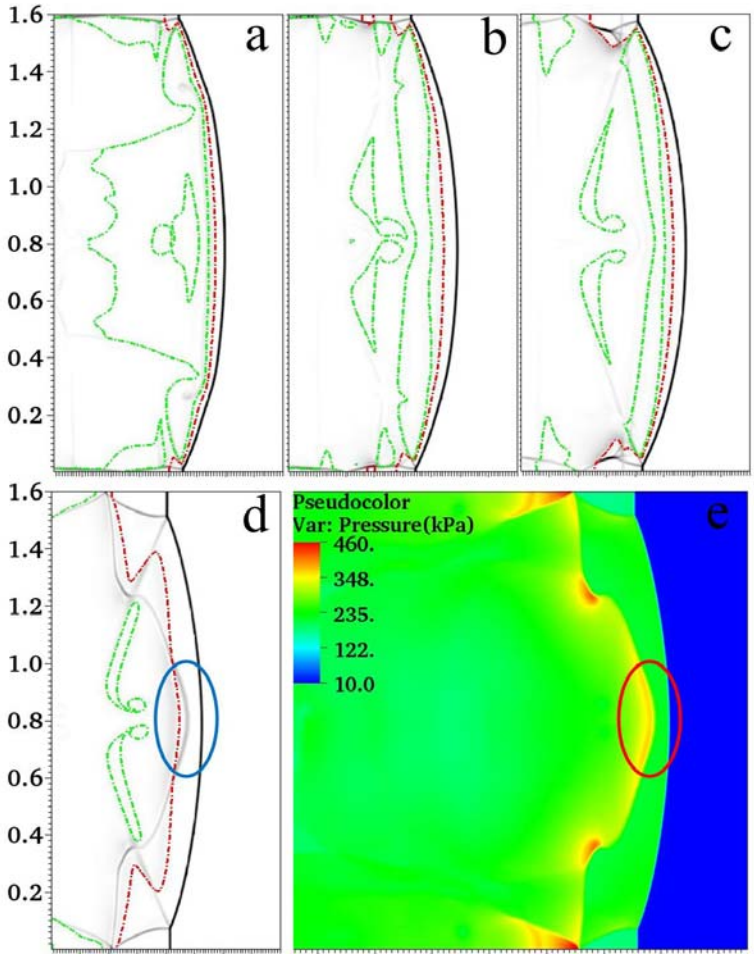

Fig.13 Density schlierens, OH isolines and pressure contour showing the evolution of the CJ detonation fronts

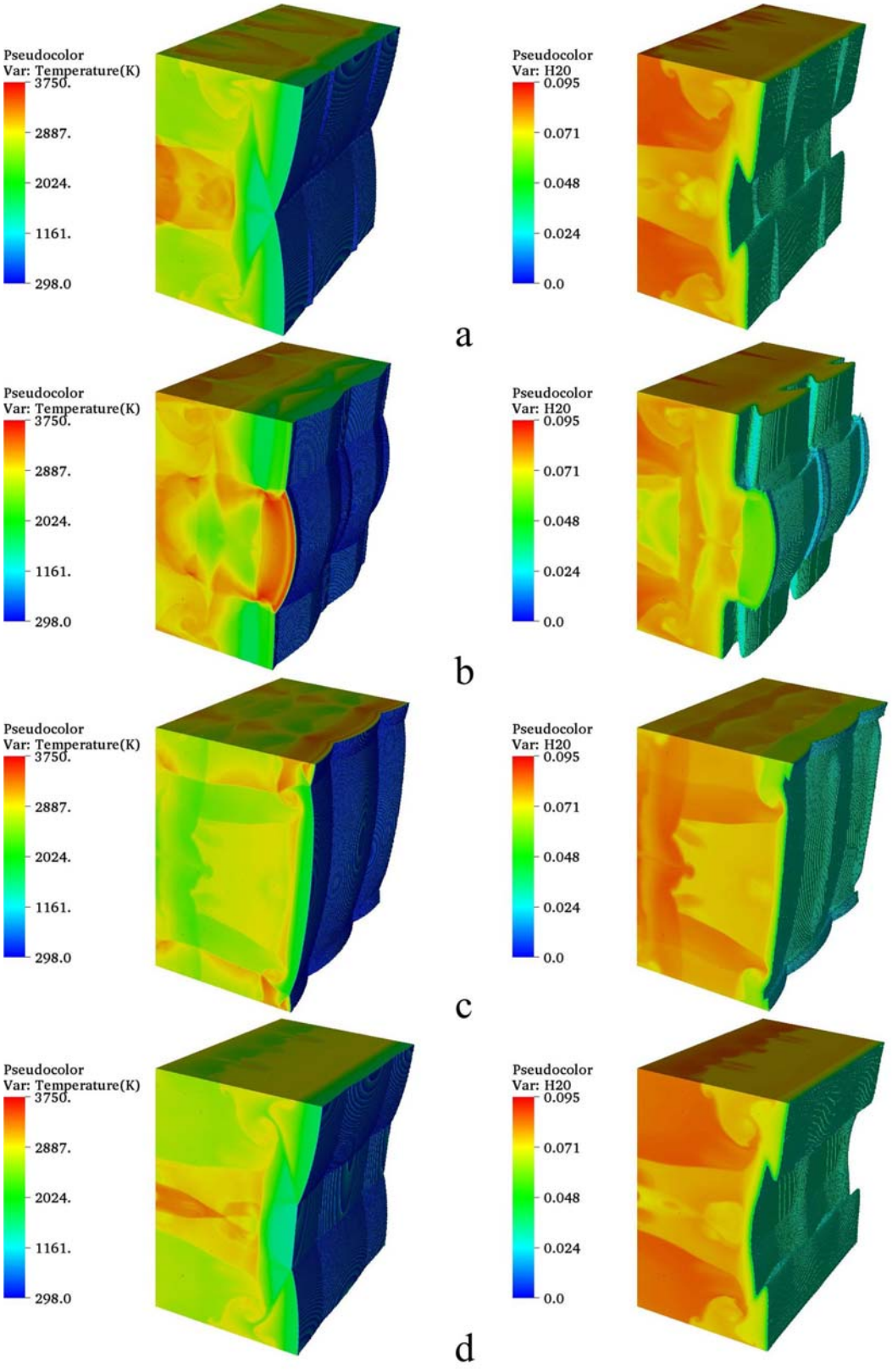

Fig.14 The cellular structures of the three-dimensional CJ detonation shown by temperature and H2O mass fraction contours. (a) t=580.0μs , (b) t=585.1μs , (c) t=590.3μs , (d) t=595.7μs

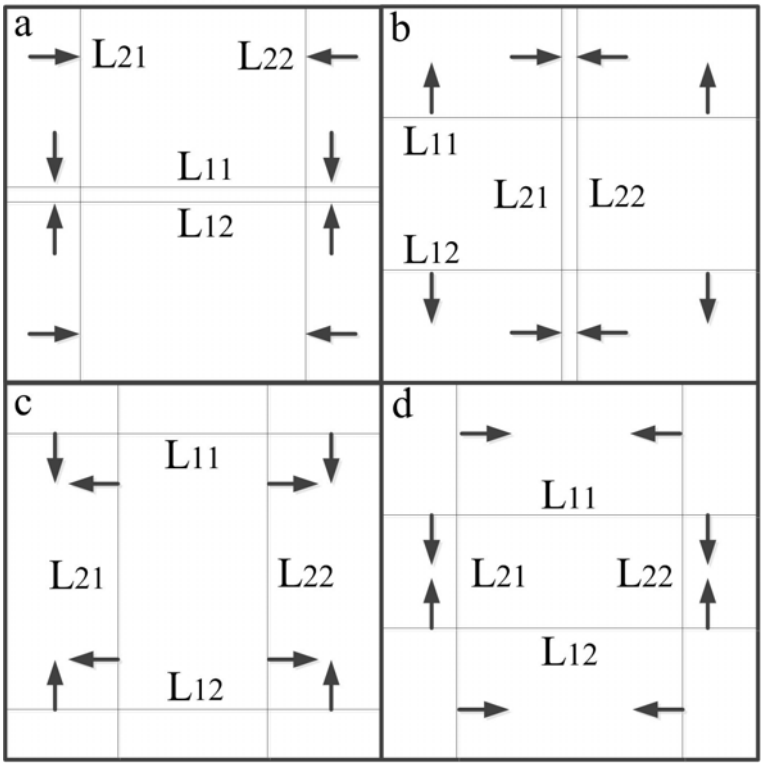

Fig.15 Schematic front view of the triple lines structure

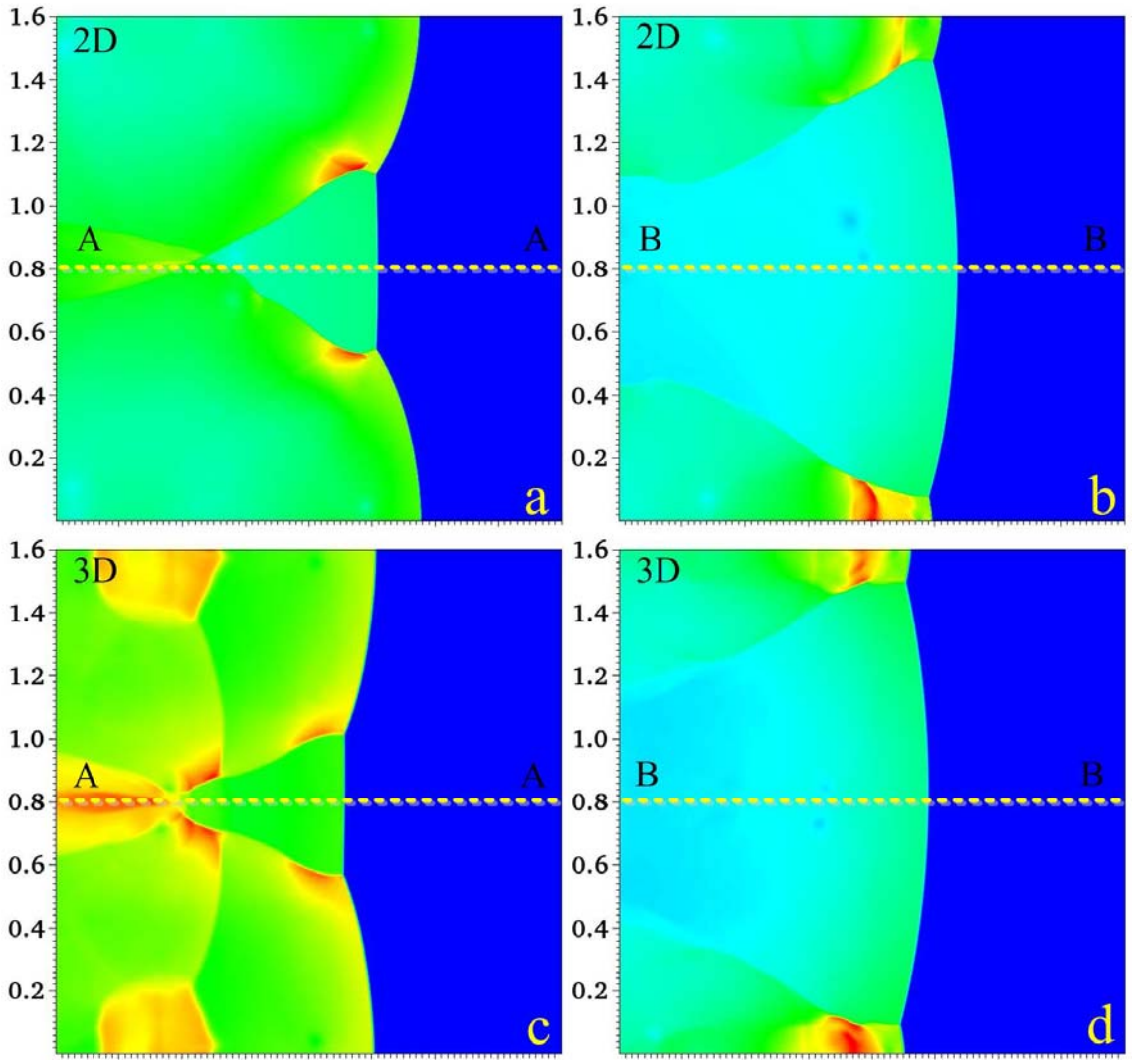

Fig.16 Comparison of instantaneous pressure and temperature distributions of two-dimensional CJ detonation and instantaneous central pressure and temperature distributions of three-dimensional CJ detonations.

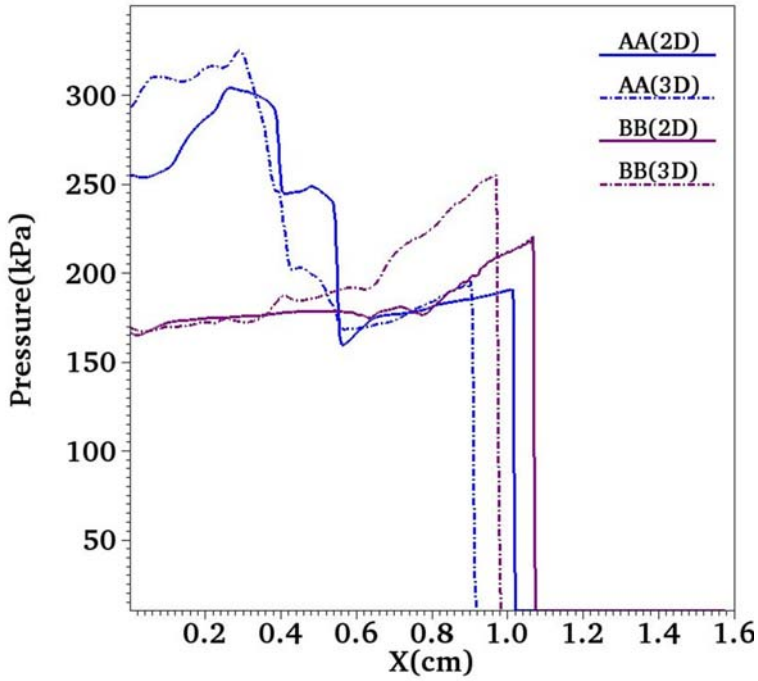

Fig.17 Comparison of instantaneous pressure and temperature distributions of two-dimensional CJ detonation and instantaneous central pressure and temperature distributions of three-dimensional CJ detonations.

List of figure captions:

Fig.1 Schematic of the calculation model

Fig.2 Temperature contours (upper) and the corresponding adaptive level distributions (lower). The mesh adaptation is five-level refinement represented by five different colors. The red color shows the highest fifth refinement level, and the blue color shows the base level. (a) t=234.1μs , (b) t=253.32μs , (c) t=272.78μs , (d) t=292.455μs

Fig.3 Front view (upper) and rear view (lower) of density isofaces and numerical schlieren images showing the initiation process using a hot jet in the three-dimensional channel. The green density isoface is at a density of $0.3\,\mathrm{kg/m^3}$. (a) t=18.85μs , (b) t=224.34μs , (c) t=323.07μs , (d) t=334.1μs

Fig.4 The OH mass fraction pseudocolors and the density isofaces (left) and the numerical schlieren images vertical to Z direction in the channel center (right). The light blue density isoface is at the density of $0.3\,\mathrm{kg/m^3}$. (a)(b) t=224.34μs , (c)(d) t=234.1μs

Fig.5 The temperature isoface (a) and the density pseudocolor (b) showing the stable bow shock surface when Z=1.6cm

Fig.6 Two-dimensional induced shock reflections for two different locations of hot jet. (a) [1.0, 1.4]cm, (b) [1.5, 1.9]cm

Fig.7 Overdriven detonation shown by the density isofaces at a density of $0.3\,\mathrm{kg/m^3}$ and numerical schlieren images. (a) t=345.35μs , (b) t=356.68μs , (c) t=368.34μs , (d) t=380.07μs

Fig.8 The reaction front represented by the OH mass fractions pseudocolors and the induction zone shown by the OH mass fraction pseudocolors and density isofaces at a density of $0.3\,\mathrm{kg/m^3}$. (a)(c) t=391.84μs , (b)(d) t=403.77μs

Fig.9 The curves of the shock front locations. (a) Two-dimensional detonation propagation;

(b) Three-dimensional detonation propagation

Fig.10 Numerical schlieren images and the corresponding OH mass fraction pseudocolors vertical to Z direction in the channel center. (a) t=391.84μs, (b) t=403.77μs, (c) t=415.74μs, (d) t=427.72μs

Fig.11 Numerical schlierens and OH contrours showing the patterns of overdriven detonation for the corresponding two-dimensional detonation. (a) t=161.13μs, (b) t=185.48μs

Fig.12 Location histories of CJ detonation fronts for the two-dimensional (a) and three-dimensional detonation (b)

Fig.13 Density schlierens, OH isolines and pressure contour showing the evolution of the CJ detonation fronts

Fig.14 The cellular structures of the three-dimensional CJ detonation shown by temperature and H2O mass fraction contours. (a) t=580.0μs, (b) t=585.1μs, (c) t=590.3μs, (d) t=595.7μs

Fig.15 Schematic front view of the triple lines structure

Fig.16 Comparison of instantaneous pressure and temperature distributions of two-dimensional CJ detonation and instantaneous central pressure and temperature distributions of three-dimensional CJ detonations.

Fig.17 Comparison of instantaneous pressure and temperature distributions of two-dimensional CJ detonation and instantaneous central pressure and temperature distributions of three-dimensional CJ detonations.